

Design and fabrication of a piezoelectric instrumented suspension for hard disk drives

Stanley Kon^a, Kenn Oldham^a, Ryan Ruzicka^b and Roberto Horowitz^a

^aComputer Mechanics Laboratory, University of California, Berkeley, CA 94720

^bHutchinson Technology Inc., 40 West Highland Park, Hutchinson, MN 55350

ABSTRACT

As data densities in computer hard disk drives increase, airflow-induced vibration of the disk drive suspension becomes a major barrier to positioning the read-write head with sufficient precision. One component in reducing these vibrations is a dedicated sensor system for detecting vibration on the sensor arm directly, which enables high-frequency sampling and modal selectivity. In this paper, an efficient method for identifying optimal position and shape of piezoelectric strain gages on a flexible structure is presented, and applied to the steel suspension of a hard disk drive. Zinc oxide deposition processes are adapted to steel substrates, and used to fabricate miniature zinc oxide strain gages at the optimal strain gage location. Substrates with sensors installed were assembled into full disk drive suspensions and tested in a commercial disk drive.

Keywords: Strain sensor, piezoelectric, ZnO, hard disk drive, suspension

1. INTRODUCTION

With areal density in hard disk drives continually increasing, future drives will require much better head positioning accuracy than current drives. The track-mis-registration budget is predicted to permit only 5 nm in 3σ root-mean-square tracking error for 500,000 tracks-per-inch (TPI) track density, which corresponds to areal density of 1 terabit per square inch. From a track following control viewpoint, the biggest barrier achieving this goal is airflow induced vibration. Windage is generated by disk rotation which excites suspension resonance modes easily, causing the read head to swing off its neutral position. The airflow-induced vibration becomes more and more dominant as bit size shrinks and disk speed increases. Traditionally, positioning is done by operating a voice-coil-motor (VCM) with feedback control. Special bits, called servo tracks, are written to the disk prior to data storage. These bits serve as landmarks for positioning and can not be overwritten by data bits. As the read head reads the data on the disk, it also periodically reads servo tracks. These readings are then fed back to the controller, which generates signals for the VCM to properly steer the E-block-suspension assembly. Schematic drawings of a hard drive and an E-block-suspension assembly are shown in Fig. 1(a) and Fig. 1(b), respectively.

Although the conventional hard drive configuration works well, there are several fundamental restrictions preventing it from meeting the required future performance. The VCM needs to be able to compensate vibration at even higher frequencies because of the smaller track widths and drive geometry. This requires a higher frequency feedback signal, which would mean more disk space wasted for servo tracks. It is also very inefficient to position the head on a nanometer scale through a centimeters-long E-block. Dual-stage servo configurations have been proposed by several researchers^{1,2,3} to make up the performance gap. Dual stage configurations utilize two actuators to better compensate vibration. The VCM is used for large and low frequency motion while a second stage miniaturized/MEMS actuator close to the head is used for small and high frequency motion. The dual stage system, however, requires high-rate vibration estimation for the controller to efficiently coordinate the two actuators. A strain sensor measuring vibration would also provide the controller with a predicted head position when position-error-signal (PES) is unavailable between two servo tracks. Suspensions incorporate strain sensors to facilitate the control of head position are called instrumented suspensions.

Previously, Li^{4,5} implemented dual stage control on hard disk drive suspensions using Lead Zirconate Titanate (PZT) transducers. Two PZT strips are attached to the suspension, one as the sensor and the other as the second

E-mail: horowitz@me.berkeley.edu, Telephone: 1 510 642 4675

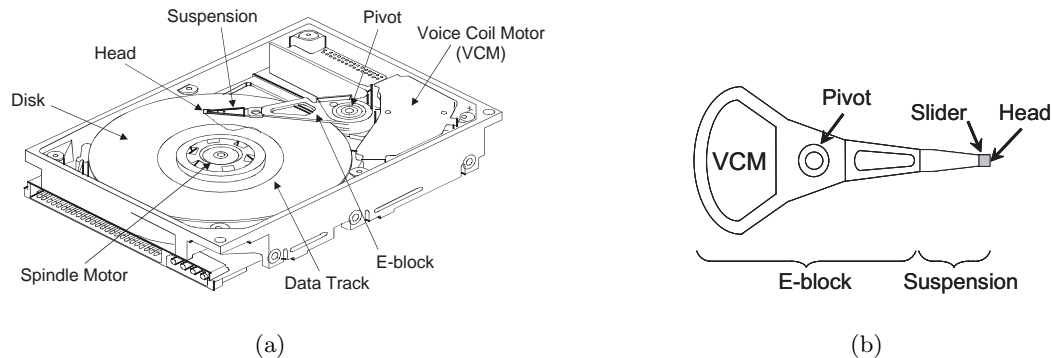


Figure 1. (a) Conventional hard disk drive configuration; (b) Conventional suspension and E-block assembly.

stage actuator. Although Li's methodology improves tracking performance, a major drawback is the size of transducers, which change the suspension dynamics and also results in a non-optimal strain signal. In designing the suspension sensors, sensor location determines what vibration modes the sensors detect. It is desirable to place sensors so that only off-track vibration information is detected for servo control. All other modes should be avoided to reduce controller load. Several researchers have proposed using an objective function based on Kalman filter results^{6,7} to optimize strain gage sensitivity to vibration on flexible structures. Kondoh et al.⁸ incorporated controller structure by minimizing the quadratic cost function in standard linear quadratic gaussian (LQG)⁹ optimal control. These solutions are optimal in terms of H_2 norm of the system, but are very computationally intensive. Oldham et al.¹⁰ introduced numerical approximations to simplify this computational complexity and applied to hard disk drive suspensions. This algorithm is further extended to design and implement sensors on the fabricated suspensions described in this paper.

In fabricating instrumented suspensions, a novel process is needed to integrate sensors and suspension fabrication. Conventionally, micro-electro-mechanical systems (MEMS) devices are built upon materials that are well-known in micro fabrication such as silicon, quartz and pyrex. The integration of micro-machined sensors onto suspensions, however, requires fabrication to be done on steel substrates. The use of steel substrates imposes a huge constraint on the process, especially processing temperatures, which makes the choice of sensor material a crucial decision. Historically, various kinds of strain sensors/gauges have been used for different sensing purposes. Piezoresistive materials are known to have good strain sensitivity. They have been integrated into devices such as pressure sensors¹¹ or atomic-force-microscopes^{12,13,14} which relate strain information to other physical properties. K. Wojciechowski et al.¹⁵ utilizes comb-finger resonant sensors to detect frequency modulated strain information. Both of the above processes requires relatively high process temperature (higher than 550 °C) to deposit films which may result in unacceptable thermal stress and alter internal properties of then steel substrates. The lithography resolution limit on steel substrates also makes comb-finger fabrication on steel wafers infeasible.

ZnO piezoelectric material can be deposited at low temperature (~ 350 °C) and are easier to deposit than PZT materials. Several researchers have used it for MEMS accelerometers¹⁶ and AFM^{17,18} strain sensing. Although the resolution of MEMS ZnO strain sensors is not documented, our calculation indicates that they are capable of resolving 100 nano-strain or better. In this paper, we incorporate the sensor location optimization with the design of ZnO piezoelectric strain sensor on an instrumented suspension. We also demonstrate the fabrication of ZnO piezoelectric strain sensors on steel substrates using MEMS technologies. The sensors show very promising sensitivities and give more vibration information than even external laser-dopper-interferometer (LDV) measurements.

2. SENSOR DESIGN

The disk drive servo system in the paper is composed of a VCM, a strain sensor and a MEMS actuator. The mechanical system is designed to achieve 5 nm (3σ) positioning accuracy in the presense of the airflow turbulence that causes suspension vibrations. Among all vibrations modes, off-track vibrations, those vibration modes causing head motion perpendicular to the data track, are especially detrimental to track following control. This off-track displacement due to vibration, labeled z , can be written as the sum of suspension vibration and MEMS actuator movement

$$z = \sum_{i=1}^n d_i \nu_i + x_{MA} \quad (1)$$

where, for the i th mode, ν_i denotes a modal coordinate, d_i denotes the displacement at the suspension tip normalized to that modal coordinate, x_{MA} denotes the MEMS actuator relative to the suspension for mode, and n denotes the number of modes considered. The modal dynamics ν_i and the MEMS actuator dynamics x_{MA} are both second order systems, subject to airflow disturbances and VCM and MEMS actuator inputs. The whole system may be normalized¹⁰ and re-written in state space form

$$\dot{x} = Ax + Bu + B_w w \quad y = C(\Phi)x + v(\Phi) \quad z = Dx \quad (2)$$

where A , B 's, and D are system matrices, u is the actuator input, w is the disturbance with spectral density w , v is the measurement noise with spectral density v , and y is the sensor strain measurement. Matrix C relates modal displacements to a measurement depending on sensor location and geometry, and Φ is a vector containing information about strain gage geometry..

To find the optimal sensor location which minimize off-track error of the closed-loop system, we minimize the H_2 norm of the system with a linear quadratic gaussian (LQG)⁹ controller.

$$\min_{\Phi} J_{H_2} = \min_{\Phi} \min_{K, F(\Phi)} E[z^T z + u^T R u] \quad (3)$$

where $F(\Phi)$ denotes the Kalman filter⁹ for a given $C(\Phi)$, and K denotes the optimal linear stationary controller. Since the VCM and MEMS actuator motions are much larger than suspension vibration, the optimization problem is solved for the case of cheap control, i.e. $R \rightarrow 0$. The optimization process is as follows: First, the optimal controller is calculated, which is independent of sensor location. Then, the matrix $C(\Phi)$ is formed for the corresponding sensor location Φ . Based on the $C(\Phi)$ matrix, an optimal linear stationary Kalman filter is found for the system. Finally, J_{H_2} is evaluated for the specific sensor location. The process is repeated throughout all sensor locations or configurations of interest. Since the optimization is computationally intensive, two assumptions are introduced to reduce computation.

1. Vibration modes are widely spread:

$$|w_i - w_j| \gg 0 \quad (4)$$

2. Sensor noise is relatively large compared to other parameters:

$$|c_{ji}| \left(\sum_{k=1}^l |b_{ik}| \right) \sqrt{\frac{w}{v}} \ll 1 \quad (5)$$

for all i and j . As described by Kenn,¹⁰ the approximation results in a simple algebraic equation for the entries in the covariance matrix M of the Kalman filter, which satisfies

$$AM + MA^T - MC(\Phi)^T v^{-1} C(\Phi) M + B_w w B_w^T = 0 \quad (6)$$

The approximate solution produces a diagonal matrix with:

$$m_{2i,2i} = m_{2i-1,2i-1} \approx \frac{w_i \sqrt{\sum_{p=1}^l b_{ip}^2} \sqrt{wv}}{\sqrt{\sum_{k=1}^r c_{ki}^2}} \quad (7)$$

The advantage of the approximation is two fold. First, it reduces computation time by at least a factor of 20. Secondly, the expression of optimization is more intuitive than brute force search, aiding in designs of complex sensor geometries.

To implement the optimization, a finite element model of the suspension to be instrumented was created, and x-, y-, and shear components of strain at various elements of the model calculated according to contribution from each mode. For example, the matrix

$$C_{\epsilon_x}(p) = [c_{x1} \ 0 \ c_{x2} \ 0 \ \dots \ c_{xn} \ 0] \quad (8)$$

describes the contributions of each vibration mode to strain in the x-direction at element p . Similar vectors for strain in the y- and shear (xy-) directions may be calculated. The $C(\Phi)$ used during optimization for a specific sensor shape is given by

$$C(\Phi) = \frac{\sum_{p \in \Phi} A_p K_s \begin{bmatrix} C_{\epsilon_x}(p) \\ C_{\epsilon_y}(p) \\ C_{\epsilon_{xy}}(p) \end{bmatrix}}{C_P + \sum_{p \in \Phi} \frac{A_p \epsilon}{t}} \quad (9)$$

with A_p the area of element p , K_s a matrix of piezoelectric coefficients in the x-, y-, and shear directions, C_P the parasitic capacitance of external leads, ϵ the permittivity of the piezoelectric film, and t the strain gage thickness. The numerator of Eq. 9 may be interpreted as charge generated in the sensor, while the denominator is a measure of capacitance. In the absence of a parasitic capacitance, strain gages would typically be located at points of greatest strain from off-track vibration modes. In more realistic models, an interesting trade-off is observed as sensor area increases, as larger sensors are more capable of overcoming parasitic capacitances that diminish sensitivity, yet the underlying strain tends to decrease as larger sensors cover areas of lower strain intensity. Good sensor shapes must will balance these effects.

Using the approximation method, many sensor locations and shapes could be quickly evaluated. Several optimal designs were selected for production, varying according to the maximum size of the sensor and permissible distance of the sensor from the suspension bend radius. Fig. 2(b) shows one optimal sensor design on the suspension, which restricting sensing elements from within 100 μm from the bend radius.

3. FABRICATION PROCESS

As shown in Fig. 2(a)(a), the strain sensor fabrication process begins by spin coating a 0.7 μm thick glass layer onto a 38 μm thick 304 stainless steel substrate. The glass layer serves as the insulation layer between the sensors and the substrate, and planarizes the steel surface, which otherwise is very rough from a micro-fabrication standpoint; it is known that a smooth surface¹⁹ is crucial to piezoelectric ZnO film growth. The glass layer also protects the steel substrate from further oxidation and maintains a smooth surface during the later ZnO deposition process. After the SOG coating, a 0.15 μm aluminum layer is deposited and patterned as the lower electrode. Then, ZnO is deposited using RF magnetron sputtering and patterned, Fig. 2(a)(b). The deposition rate at 350C with 200W forward power, 35 mTorr oxygen and 35 mTorr argon is approximately 0.8 μm per hour. A 0.8 to 1 μm ZnO film is sufficient to show good piezoelectric properties. Another SOG layer is then spin-coated and patterned for insulation, Fig. 2(a)(c-d). A second aluminum layer is evaporated and patterned to form the other electrode, Fig. 2(a)(e). Finally, the last SOG is coated for passivation, Fig. 2(a)(f).

Once the fabrication of sensor itself is completed, additional steps are needed to transform the substrate into small pieces that will be incorporated into the suspension assembly process. First, the SOG layers are etched away using reactive-ion-etching(RIE) except the portion that encapsulates the sensors and the leads, Fig. 2(a)(g). An SF_6 plasma attacks oxide selectively, stopping automatically at the steel surface. Second, the substrate is coated with a thick photoresist layer on both sides and patterned on the side containing strain sensors. Similar to silicon bulk micromachining, the substrate is then etched in a FeCl_3 solution to form small steel pieces, Fig. 2(a)(h). After etching, each of these steel pieces, called hinges, is welded together with other parts to form a complete suspension assembly. Finally, the assembly is bend at a pre-designed location to ensure a correct gram load once it is loaded onto the disk.

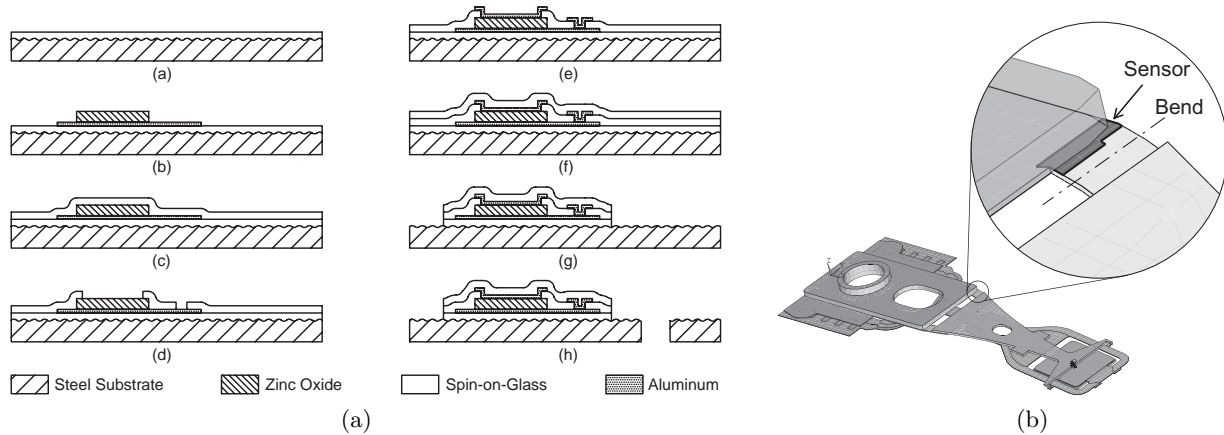


Figure 2. (a) Fabrication process flow for instrumented suspensions; (b) A sensor design on the suspension using the optimization theory.

4. TESTING AND DISCUSSION

4.1. Circuit

Although ZnO is made compatible with steel substrates, its piezoelectric constants are at least an order of magnitude smaller than PZT. In other words, ZnO produces much less charge than PZT when subjected to the same amount of external strain. Micro scale piezoelectric sensors generate even less charge, as piezoelectric sensors generate charge proportional to their dimensions. Hence, a proper interface circuit for signal amplification is crucial for vibration signal retrieval. It is also desirable to place the circuit very close to the sensor to minimize environmental noise and feed-through. Fig.4(a) shows the suspension and the circuit installed on a hard drive E-block.

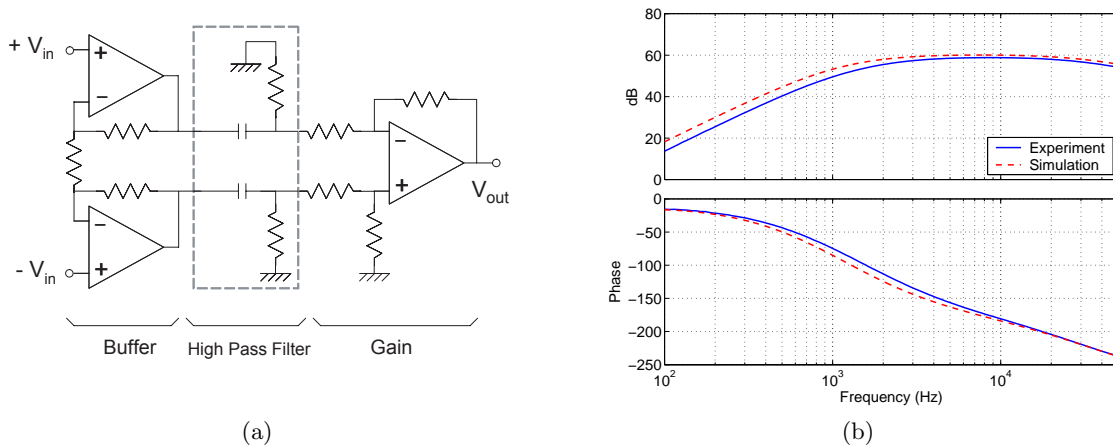


Figure 3. (a) Circuit topology of the interface circuit; (b) The experimental and simulated transfer function from circuit input to output.

Since the suspension vibration modes of interests are between 1 kHz and 30 kHz, it is beneficial to build a circuit that only amplifies signals at this frequency range. This will minimize the noise from other frequencies and also reduce the probability of circuit saturation from unwanted disturbance. The circuit is composed of two stages, a buffer stage and a gain stage, as shown in Fig. 3(a). The buffer stage utilizes a differential input to

reduce the common mode noise from both leads with gain of 100. The relatively large gain at the first stage is desirable so as to amplify the signal and increase signal-to-noise ratio(SNR) using minimal circuitry. The second stage is a differential-to-single-end converter with gain of 10. During testing, maximum circuit gain from input to output is found to be 870, although the simulation shows the number to be 1000, shown in Fig. 3(b). A high pass filter is added between the two stages to prevent low frequency noise from being amplified.

4.2. Experimental Setup

Due to the limited space inside hard disk drives, surface mount components were used to build the interface circuit directly onto the drive's E-block. The operational amplifier and components were glued to a centimeter square chip and connected by wire bonding, Fig. 4(a). Once the suspension is attached to the E-block, sensor signals are wired to the circuit through the drive's flex circuit and the amplified signals are passed to the connection pins at the back side of the drive. A dummy MEMS micro actuator and a dummy slider were installed on the suspension for the correct mass load. The dummy actuator is a gap-closing actuator which is designed for this particular dual stage control system.²⁰ The actuator is intentionally glued so as to be immobile during the experiments, so that its dynamics do not show up in the measurements. Fig. 4(b) shows a close view of the hinge area where the sensors are located. The sensors fabricated on the test suspension assembly utilizes the design shown in Fig. 2(b) with $95,924 \mu\text{m}^2$ in area and $0.8 \mu\text{m}$ thickness. Two LDVs are used to measure head off-track and/or non-off-track displacement. The LDVs are set to displacement mode with a $0.5 \mu\text{m}/\text{V}$ conversion factor. All measurements in this paper are taken without a disk installed for ease of measurement.

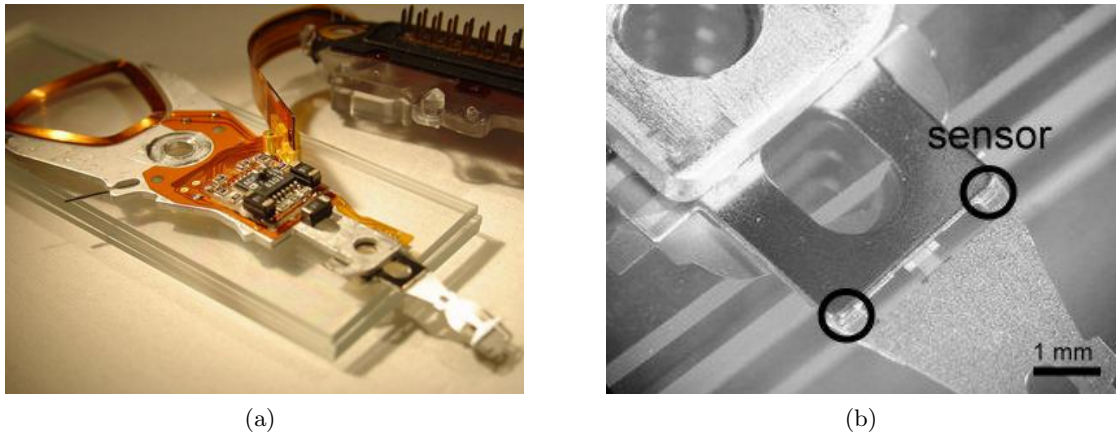


Figure 4. (a) The E-block and suspension assembly with interface circuit attached; (b) A close view of the tested sensors.

4.3. Results and Discussion

4.3.1. LDV and Sensor Signal Comparison

Several measurements were taken in order to examine the differences between LDVs and sensor response. An HP35665A analyzer is used to measure the suspension system dynamics from VCM to read head off-track and non-off-track displacement. The analyzer applies a 10 mV excitation signal on the VCM, sweeping from 100 Hz to 50 kHz. At the same time, the LDVs measure the head displacement, which is also fed to the analyzer. A total of 501 measurements are taken at each frequency point with 25 cycles averaging and settling time. The experiment is performed when the disk spindle is off. This reduces uncertainties such as RF noise feed-through and spindle induced vibration. Both off-track and non-off-track measurements are taken. The resulting transfer functions are shown in Fig. 5(a). A second experiment is performed to measure the transfer function from VCM to the sensor. The experiment settings are the same as the previous experiment except that, instead of the LDV signals, the amplified sensor signal is recorded. The transfer function from VCM to circuit output is shown as the solid line in the upper half of Fig. 5(b).

The measured resonance modes are superimposed on different underlying dynamics. The resonance modes in the LDV plots ride on 40 dB/dec roll-off curves, which are the rotational rigid body mode of the suspension

assembly in the off-track and non-off-track direction, whereas the resonance modes in the sensor plot ride on the circuit gain curve, which is scaled down and shown as the dashed line in Fig. 5(b). In spite of this, the resonance modes measured by the sensor is very similar to those measured by the LDVs. It is found that the vibration modes in the sensor measurement are the union of those modes detected by the two LDV measurements. This is reasonable because the sensor is located at the most flexible part of the suspension, where the strain tends to be concentrated. Furthermore, the sensor optimization procedure is expected to choose a location giving large response from off-track response. The LDVs, on the other hand, only detect vibration modes for which vibration motions are parallel to the direction of the laser beam. Torsional modes, such as the mode around 700 Hz, may be partially picked up by both LDV measurements. The plots also indicate that the sensor has better signal-to-noise ratio than the LDVs, especially at frequencies higher than 1 kHz. The fluctuation shown on the LDV measurements at this frequency range does not appear in the sensor measurement, even though the gain of the sensor interface circuit is at its maximum in this range.

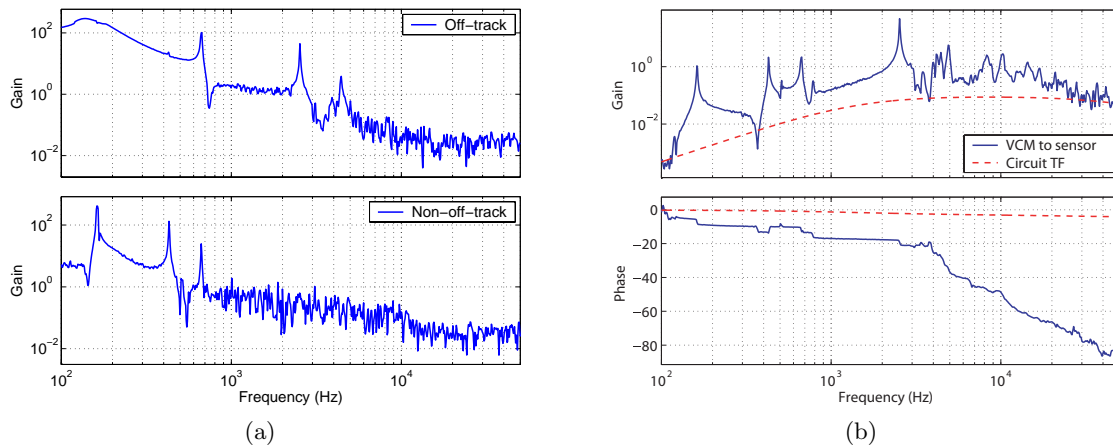


Figure 5. (a)Top: The transfer function from VCM to off-track (horizontal) LDV signal. Bottom: The transfer function from VCM to non-off-track (vertical) LDV signal; (b) The transfer function from VCM to the amplified sensor signal and circuit gain. Circuit gain is down shifted by a factor of 10,000 to fit into the plot.

4.3.2. Model Verification

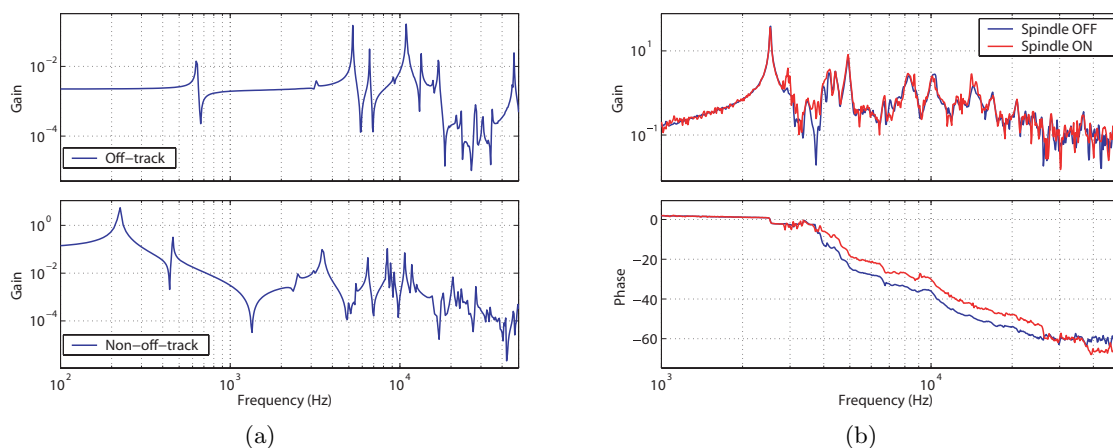


Figure 6. (a) Simulated sensor strain subjected to off-track (top) and non-off-track (bottom) excitation; (b) Transfer function measurements from VCM to the amplified sensor signal with spindle motor turned on (solid line) and off (dotted line).

Since the sensor location optimization theory relies on an optimal dual-stage controller, of which the design is based on the modelled suspension dynamics, we intend to compare the model and the fabricated suspension dynamics. This would help us identifying problems and evaluating closed-loop system performance in the future. While sensor optimization was performed on a suspension model loaded with a disk, we evaluate model accuracy by comparing sensor experimental results to a finite element model of the unloaded suspension. The simulation was carried out by applying excitations at the base of the suspension model in off-track and non-off-track direction, respectively, and evaluating strain at the sensor location. The simulated transfer function from off-track excitation to the strain is shown in the top half of Fig. 6(a) and the transfer function from non-off-track excitation to the strain is shown in the bottom. It is found that most of the vibration modes in the non-off-track transfer function, Fig. 6(a), also appear in the sensor result, Fig. 5(b). The modes in the sensor experimental result are slightly lower than those in the simulated plot as the suspension was overetched during fabrication, resulting smaller spring constants for each mode. The modes in sensor experimental result appear to be even lower than the corresponding modes in the simulated non-off-track transfer function, except the torsional mode at 635 Hz. It is suspected that the effective moment of inertia for off-track motion is particularly susceptible to hinge overetching which essentially lower the spring constants for these modes.

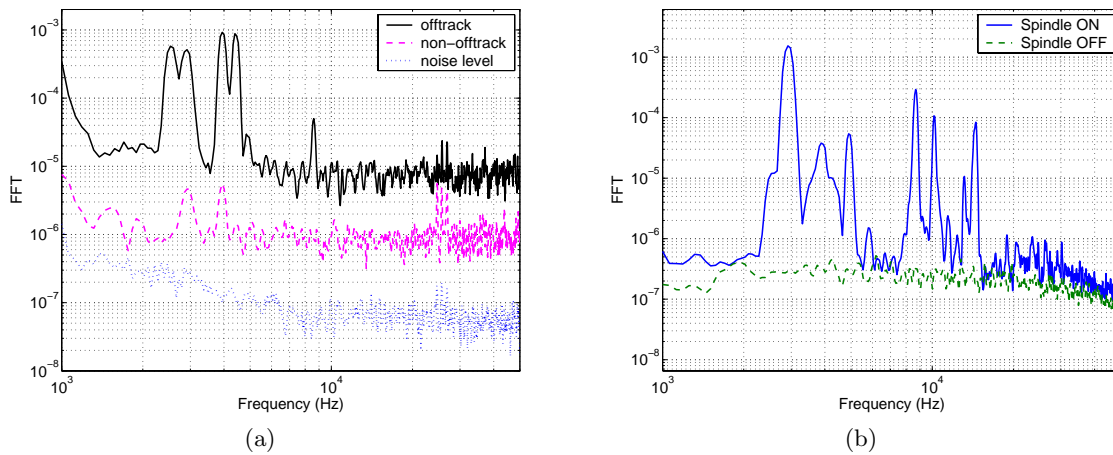


Figure 7. (a) Fast Fourier transform of the horizontal and vertical LDV signals and the LDV noise level with spindle motor turned on;(b) Fast Fourier transform of the amplified sensor signal and noise level.

4.3.3. Effects of the Spindle Motor

The ZnO strain sensor can be vulnerable to environmental noise. For instance, a fluorescent light located one meter above the experimental setup was found to influence the noise level of sensor signals once the light turned on. As our calculation indicates that the sensor generates only sub-picoampere current during measurements, it is speculated that the electromagnetic noise generated by the spindle motor may dominate the sensor signal. However, with the spindle motor turned on, a transfer function measurement from VCM to the sensor shows that the spindle motor has only minor effects on the resulting transfer function, as shown in Fig. 6(b). There is a slight discrepancy between 3 and 4 kHz. To examine this, four more measurements were taken with the spindle motor turned on. With no driving signal applied to the VCM, LDV is used to measure the off-track motion, non-off-track motion and the noise level. The fast-Fourier-transform(FFT) of the signals are shown in Fig. 7(a). Note that, in order to make the figure easy to read, the off-track and non-off-track curves are shifted away from the noise level. The sensor signal was also measured and its FFT is shown in Fig. 7(b). Comparing these two plots and the gain plot of VCM-to-sensor transfer function, Fig. 5(b), all those peaks appearing in the sensor signal FFT measurement, Fig. 7(b), also appear in at least one of the other two plots. This indicates that the sensor signal in Fig. 7(b) results from suspension vibration modes which are excited by spindle rotation. These modes either are detected by LDV measurements or can only be detected easily using the sensor. If the sensor signal were caused by the feed-through of spindle or any other kind of noise, their modes would not coincide with

all the suspension resonance modes. The conclusion leads us to believe that the discrepancy in Fig. 6(b) is in reality a mechanical vibration mode excited by the spindle motor.

4.3.4. Fabrication Issues

As mentioned in Sec. 3, each suspension is plastically deformed during manufacturing to insure that a correct force is pre-loaded onto the disk after disk installation. The deformation is applied by rolling the hinge against a bend of about few hundred microns in radius. Unfortunately, the hinge is also the place where the sensors are fabricated. Due to a limited space on the hinge, it is inevitable that the bend is located close to the sensor. As a result, cracks on the strain sensor are usually observed after applying the bend. The severity of the cracking depends on the distance between the sensor and the bend. Sensors simply peel away if the bend is applied directly on the sensor, whereas only a few visible cracks are observed if the bend is located 200 μm away from the sensor. Our tests show that most cracked sensors still show decent piezoelectric response. As the ZnO is covered by a non-transparent aluminum electrode and SOG layers, all the cracks observed are those appear on the SOG layers. The top aluminum electrode is ductile and does not show any cracks. Further examinations are required to detect cracking of the ZnO film, which may reduce strain sensor sensitivity, and to which the measured response is directly related.

5. CONCLUSION AND FUTURE WORK

Strain sensors on an instrumented disk drive suspension are designed using the approximation of the cost function of LQG controllers by incorporating piezoelectric characteristics into the optimization algorithm. ZnO sensors designed by this procedure have been fabricated directly on steel substrates successfully. The fabricated substrates are transformed into suspension components using bulk micromachining and are assembled into hard disk drive suspensions. The sensors show remarkable response even in the presence of environmental noises. It is found that sensor signals have better signal-to-noise ratio and contain more vibration information than LDV measurements.

Further examination is needed to investigate cracking as a result of applying a bend to the suspension part. To make the system more robust, new sensor designs are needed with additional constraints to keep the sensor away from the bend. Other piezoelectric materials may also be tested with current sensor design.

6. ACKNOWLEDGMENTS

The work is supported by National Science Foundation (NSF), Information Storage Industry Consortium (INSIC), and Computer Mechanics Laboratory (CML).

REFERENCES

1. R. Oboe, A. Beghi, and B. Murari, "Modeling and control of a dual stage actuator hard disk drive with piezoelectric secondary actuator," *Proc. IEEE/ASME Intl. Conf. Adv. Int. Mechatronics*, pp. 138–143, September 1999.
2. R. Evans and M. Karaman, "Closed loop testing of a suspension based piezoelectric microactuator," *Digest of the APMRC 2000*, pp. WA201–WA202, November 2000.
3. L. Guo, D. Martin, and D. Brunnett, "Dual-stage actuator servo control for high density disk drives," *Proc. IEEE/ASME Intl. Conf. Adv. Int. Mechatronics*, pp. 132–137, September 1999.
4. Y. Li, R. Horowitz, and R. Evans, "Vibration control of a pzt actuated suspension dual-stage servo system using a pzt," *IEEE Transactions on Magnetics* **39**, pp. 932–7, March 2003.
5. Y. Li, F. Marcassa, R. Horowitz, R. Oboe, and R. Evans, "Track-following control with active vibration damping of a pzt-actuated suspension dual-stage servo system," **3**, pp. 2553–9, IEEE, 2003.
6. K. Hiramoto, H. Doki, and G. Obinata, "Sensor/actuator placement for vibration control using explicit solution of algebraic riccati equation," *J. Sound and Vibrataion* **229**(5), pp. 1057–1075, 2000.
7. J. Juang and G. Rodriguez, "Formulations and applications of large structure actuator and sensor placements," *Proc. YPI&SU/AIAA Symposium on Dynamics and Control of Large Flexible Spacecraft*, pp. 247–262, 1979.

8. C. Y. Kondoh, S. and K. Inoue, "The positioning of sensors and actuators in the vibration of flexible systems," *JSME Int'l J.* **33**, pp. 145–152, 1990.
9. P. J. Antsaklis and A. N. Michel, *Linear Systems*, McGraw-Hill, 1998.
10. K. Oldham, S. Kon, and R. Horowitz, "Fabrication and optimal strain sensor placement in an instrumented disk drive suspension for vibration suppression," *Proceeding of the 2004 American Control Conference* , pp. 1855–1861, 2004.
11. W. P. Eaton and J. H. Smith, "Micromachined pressure sensors: review and recent developments," *Smart Materials & Structures* **6**(5), pp. 530–539, 1997.
12. F. J. Giessibl and B. M. Trafas, "Piezoresistive cantilevers utilized for scanning tunneling and scanning force microscope in ultrahigh vacuum," *Review of scientific instruments* **65**(6), p. 1923, 1994.
13. A. J. Brook, S. J. Bending, J. Pinto, A. Oral, D. Ritchie, H. Beere, M. Henini, and A. Springthorpe, "Integrated piezoresistive sensors for atomic force-guided scanning hall probe microscopy," *Applied physics letters* **82**(20), p. 3538, 2003.
14. M. Tortonese, R. C. Barrett, and C. F. Quate, "Atomic resolution with an atomic force microscope using piezoresistive detection," *Applied physics letters* **62**(8), p. 834, 1993.
15. K. Wojciechowski, B. Boser, and A. Pisano, "A mems resonant strain sensor operated in air," *Micro Electro Mechanical Systems, 2004. 17th IEEE International Conference on* , pp. 841–845, 2004.
16. P. L. Chen, R. D. Jolly, G. L. Halac, R. S. Muller, R. M. White, A. P. Andrews, T. C. Lim, and M. E. Motamedi, "Integrated silicon microbeam PI-FET accelerometer," *IEEE Trans. Electr. Devices* **ED-29**(1), pp. 27–33, 1982.
17. T. Itoh and T. Suga, "Development of a force sensor for atomic force microscopy using piezoelectric thin films," *Nanotechnology* **4**(4), pp. 218–224, 1993.
18. T. Shibata, K. Unno, E. Makino, Y. Ito, and S. Shimada, "Characterization of sputtered zno thin film as sensor and actuator for diamond afm probe," *Sensors & Actuators A-Physical* **A102**(1-2), pp. 106–113, 2002.
19. J. B. Lee, S. H. Kwak, and H. J. Kim, "Effects of surface roughness of substrates on the c-axis preferred orientation of zno films deposited by r.f. magnetron sputtering," *Thin Solid Films* **423**(2), pp. 262–266, 2003.
20. K. Oldham, X. Huang, and R. Horowitz, "Design, fabrication and control of a high-aspect ratio microactuator for vibration suppression in a hard disk drive," *Proceedings of the 16th IFAC World Congress* , 2005.